Journal of
Sensor and Actuator Networks

MDPI

Article

A Sensor to Monitor Soil Moisture, Salinity, and Temperature Profiles for Wireless Networks

Xavier Chavanne * and Jean-Pierre Frangi

Institut de Physique du Globe de Paris, Université Paris Cité, UMR 7154 CNRS, F-75205 Paris, France; frangi@ipgp.fr
* Correspondence: xavier.chavanne@u-paris.fr

Abstract: This article presents a wireless in situ sensor designed to continuously monitor profiles of parameters in porous media, such as soil moisture, salinity, and temperature. A review of existing in situ soil sensors reveals that it is the only device capable of measuring the complex permittivity of the medium, allowing for conversions into moisture and salinity that are independent of the instrument. Flow perturbation and invasiveness have also been minimized to maintain good representativeness. Plans include autonomous networks of such sensors, facilitated by the use of the recent radio mode LoRaWAN and cost optimizations for series production. Costs were reduced through electronic simplification and integration, and the use of low-cost modular sensing parts in soil, while still maintaining high measurement quality. A complete set of sensor data recorded during a three-month trial is also presented and interpreted.

Keywords: wireless networks of in situ sensors; continuous monitoring; sensor for soil moisture and salinity profiles; temperature profiles

Citation: Chavanne, X.; Frangi, J.-P. A Sensor to Monitor Soil Moisture, Salinity, and Temperature Profiles for Wireless Networks. *J. Sens. Actuator Netw.* **2024**, *13*, 32. https://doi.org/10.3390/jsan13030032

Academic Editor: Lei Shu

Received: 12 April 2024
Revised: 13 May 2024
Accepted: 23 May 2024
Published: 27 May 2024

1. Introduction

Economic activities (in agriculture and engineering) and environmental studies (hydrology, climate) require in situ continuous monitoring of water content and other variables in a porous medium such as soil. Soil moisture is a central element in the hydrological cycle and energy balance among the atmosphere, plant, and subsoil [1–3]. Water in soil is replenished by precipitation, drains toward deeper horizons, and is absorbed by sunlit plants for their growth and to regulate their temperature through transpiration. Vegetation activity controls the local climate by its capacity to absorb a large part of incoming solar radiation without overheating, thanks to water evaporation. However, for this process to occur and for plants to thrive, they depend on the availability of water in the soil. As a result, the soil should act as a storage providing a first and rapid buffer to maintain an equilibrium between the energy and water fluxes at the soil–atmosphere interface over time and under changing atmospheric conditions. If the soil becomes saturated due to excessive rainfall, ponding and runoff occur at the surface, which may lead to catastrophic flooding. Conversely, a lack of water causes plants to be unable to cope with incoming radiation, resulting in stress and withering. Consequently, maintaining sufficient water content is also of paramount importance in agriculture, especially when irrigation is necessary, as fresh water is becoming increasingly scarce [4,5]. In addition to the total amount of water in soil (over the horizon of plant roots), the knowledge of its vertical profile will provide more details about the distribution and offer insights into the vertical water fluxes occurring from the surface over time.

Given its role in the energy and water balances, monitoring soil temperature and its profile is also relevant on intra-day and annual scales, as well as during the year [6]. Time series of the temperature vertical profile at one point, using the equation of heat diffusivity, allow for the determination of the soil's thermal properties (heat capacity, thermal conductivity, etc.), which in turn enables the assessment of quartz fraction [7]

or even water content or flux [8]. Moreover, because temperature controls chemical and bacterial activities, it plays a role in the capacity of the plant root system to absorb water and nutrients. In very cold climates, both soil temperature and the content of liquid water are critical for studying the extent and evolution of permafrost, which is part of the soil that remains permanently frozen, influenced by the changing climate or the presence of a flowing river [9].

This set of basic soil variables would not be complete without considering the water salinity in the soil, which is deduced from monitoring the soil's bulk conductivity and its water content [4,10]. This indicates the presence of nutrients or the intrusion of highly saline or even contaminated water from rising groundwater. Such information can guide the timing, duration, and intensity of actions needed to control nutrient deficiencies or manage rising saline water in the root zone.

We can also highlight the importance of monitoring water content in concrete during its manufacture to ensure good quality [11], or during its aging with permanent electrodes. There are additional applications for silos and even compost [12]. Monitoring temperature is also important for these processes. These materials often exhibit high salinity, which can pose challenges for moisture measurement with electronic circuits. Because these operations typically involve batches of relatively good homogeneity, only one sensor is required per batch or series of production with identical parameters. Electrodes can be recovered or separated from the electronic circuits of the sensor for reuse.

Continuously monitoring certain quantities requires defining the temporal resolution of the operation, which includes the measurement frequency and the span of time for data recording. These parameters depend on the phenomena under study. Understanding how a small catchment responds to rare but intense rainfall necessitates very high instrument sampling, at least every 5 minutes, to measure the rate of water infiltration in the soil. On the other hand, observing the influence of climate change on this catchment will require a long series of data spanning several years [1].

Another challenge of monitoring soil variables is their spatial variability, which can arise from factors such as lateral changes in soil characteristics, localized or uneven water supply to the soil—even from rainfall—and variations in field or catchment morphology, such as slopes, etc. Section 2 provides insights into the diverse measurement techniques used to address this issue, depending on whether a simple average over several kilometers is sufficient or if detailed variability information is required.

Before presenting our recent generation of sensors to address these various applications and their requirements, in Section 2, we carry out a review of past and recent developments of in situ soil sensors for wireless networks. There are detailed challenges and limitations encountered, particularly the difficulties in reconciling cost reduction with measurement quality. This review explains choices made for the development of our own sensors. In the third section, the main features are described with evolution from previous generations of prototypes. Maintaining high measurement quality remains a primary objective for our sensors. We employ a strategy that integrates design optimization with some compromises to reduce costs and produce a demonstrator for series production. The entire instrument is modeled based on circuit theory to identify and correct all potential biases. This approach allows us to anticipate factors responsible for sensor-to-sensor variability, particularly by utilizing component specifications and reducing them.

All data from a prototype trial are provided in the fourth section to demonstrate its capability as a multivariable, multi-horizon wireless sensor.

2. Review of Sensors for Monitoring In Situ Soil Variables

2.1. Why an In Situ or Local Sensor Rather than an Integrative Approach?

To address these challenges, the solution presented in this article relies on the networks of in situ sensors. The sensor itself uses a probe inserted into the soil to determine its water content and other soil variables. It samples the volume around it, of which, the scale may be as low as a few cm^3. Having a vertical profile requires the use of three or more probes

along a medium depth. Moreover, for the continuous monitoring of water content in soils, only indirect methods are realistic as detailed further. As a consequence, the sensor output, without careful consideration of the measurement technique, can be influenced by other factors such as sensor temperature, soil salinity, or texture. Hence, this approach has been criticized for lack of representativeness, device invasiveness, potential biases, and high costs, including those of installation and maintenance, especially for agricultural use [13]. In this regard, non-invasive methods can be considered; these methods integrate over an area ranging from 200 m to several kilometers, such as field counters of neutrons produced from cosmic rays and back-scattered by H atoms of water [14], or space- or airborne radiometers based on surface temperature or emissivity [15]. Their response delay or time resolution ranges from at least one hour to several days. Their measurement principle is more indirect than those of in situ sensors, and their unique output is influenced by cloud contamination, vegetation cover, air humidity, and moisture distribution at the same water amount, among other factors. The depth of soil probed depends on water content and can be as shallow as 1 cm in the case of radiometers. These instruments require in situ calibration, often provided by networks of in situ sensors. When considering all costs, including those for autonomy (data retrieval, energy, operations) and maintenance (including regular calibration), setting up a network of in situ sensors can be less expensive.

Moreover, in situ sensors spread over the area of interest will not only give average values of the soil variables but also inform about patterns of soil moisture, either for studies of the local climate in a small catchment [1] or to allow improving irrigation spatial efficiency [16]. Without the need for spatial mapping, in situ sensors are more appropriate for applications such as controlling infrastructure stability, monitoring concrete aging, assessing silo conditions, and tracking compost maturation. In situ sensors are not a perfect solution, but alternatives are not ideal either.

2.2. Communication Mode for Remote Monitoring

As a first requirement, managing multiple sensors at different places should be facilitated by wireless data transfers from each sensor toward a unique center or database on the Internet with easy access.

Since the beginning of this century, progress in telecommunications (such as mobile cellular networks, Internet development, and further miniaturization of circuits) has led to attempts at creating such wireless networks [17]. In some German catchments, the SoilNet network, consisting of several hundred devices spread over less than 1 km^2, was implemented under the Terrestrial Environmental Observatories (TERENO) program [18]. A modular approach was chosen for designing each device, which comprises about six probes installed in a trench in the soil—two at each depth. These probes, manufactured by Meter Group (formerly Decagon), are connected at the surface to a processing circuit and a radio module. The communication mode is derived from the Zigbee protocol with a range of less than 100 meters, similar to other short-range modes such as Bluetooth-LE and WiFi. Another drawback of these modes is their high power consumption, typically associated with an unnecessarily large transfer band, although Zigbee represents an improvement over others.

The idea gains further traction with the recent emergence of communication modes that overcome the drawbacks of previous ones, such as Low Power Wide Area Networks (LPWANs) like Long Range Wide Area Networks (LoRaWANs) [19]. In 2023, worldwide shipments of LPWAN chipsets, excluding China, reached approximately 200 million units, with an annual growth rate of more than 20%. Since 2015, LoRaWAN has been an open standard for radio communication, utilizing license-free bands in the sub-gigahertz frequency range. Moreover, it is supported internationally by a large alliance of corporations, ranging from semiconductor foundries to telecommunication operators. Another LPWAN mode promoted by operators of cellular networks is NB-IoT (Narrowband Internet of Things). While it also promotes LTE for larger throughput, it comes with higher consumption. NB-IoT operates on the frequency band of the 4G mobile network. Common points

between LPWAN modes include their long range between the emitter and receptor, which can exceed 10 km in rural areas, and low power consumption for sending messages. For example, a 40-byte payload with a LoRaWAN module requires between 100 mJ (for the lowest time on air but highest loss rate) to 380 mJ (for the highest time on air) [20]. The radio transceiver and processor are integrated into a surface mount module, priced around 15 $. Moreover, the base station or gateway that forwards the data to the internet can support more than one thousand sensors (also known as nodes) in a simple star configuration. The main trade-off is a latency of a few seconds, a duty cycle of around 2% (in the case of license-free bands), and the reduced bandwidth of their communication mode, which limits the amount of data sent. These constraints do not impact the operations of most sensors. In the case of LoRaWAN, 40 bytes of data can be transferred in a message every minute, and this quantity can be increased when the signal quality between the node and gateway is good enough. The data in a message sent by the sensor presented in this article represent three soil variables with high resolution (16 bits) retrieved from three to five depths, along with some parameters of the circuits to check their functioning.

The advantages of LPWAN modes, along with new developments in the Internet such as cloud computing and open-source software, have made their use for monitoring soil status essential. This has compelled legacy manufacturers of soil moisture sensors, such as Campbell Scientific and Meter Group (formerly Decagon), to adapt their offerings by incorporating means to transfer sensor data through an LPWAN. For example, Campbell Scientific has commercialized the ASPEN 10, a data logger for its sensors that operates with NB-IoT. Recently, very simple and low-cost probes have appeared, consisting of a blade-shaped printed circuit board (PCB) that can be inserted into the soil [21]. The specifications of its power supply and output are suited to standard electronic circuits equipped with an LPWAN module, such as Arduino.

2.3. Requirements for the Sensor

In this article, a probe refers to the sensing component inserted into the soil to measure one or more variables at one or multiple depths, depending on the probe design. The frame of the probe may include the measuring circuit along with the electrodes, like the PCB-based probe mentioned above. An instrument comprises the probes and the electronic circuit necessary to obtain the profile of a variable. It requires energy and provides an output to be transferred. The device includes all instruments, the electronic circuits for control and communication, the housing, and the power supply to be autonomous. It corresponds to the node of a wireless network. The term sensor is loosely defined and can represent any of these different terms. The next step in the development of wireless networks of in situ sensors is the industrial-scale production of the sensors themselves. Mass-producing identical sensors will lower costs and increase their appeal. However, the prototype must be cost-effective, designed with off-the-shelf components, a reduced number of parts, and different models. Assembly and quality control should be streamlined to reduce labor costs. Instruments must provide an output that can be easily digitized, such as a direct voltage or a periodic signal. The entire device must be self-sufficient in terms of energy, processing, and communication to operate for at least one year without intervention. Other constraints include robustness for long-term field operations with minimal maintenance and compactness for ease of installation. Indeed, the total device cost includes not only production but also installation, field operation, and maintenance costs. There is a necessary trade-off between fabrication costs and all these constraints.

Furthermore, 'low cost' may be synonymous with low measurement quality, depending on the desired level of accuracy. Measurement quality involves three criteria: an accurate measurement technique to output the intended variable, sufficient soil sampling volume, which depends on probe geometry, and the overall device geometry to minimize any perturbation of water flows above and below ground. The soil water content Θ_v deduced at the probe location should be representative of the moisture at a distance (about 50 m) in the case of low-sloped homogeneous soil. It is important to note that two

sensors can have the same probe geometry, such as a blade-shaped PCB or electrodes along a cylinder, but use different measurement techniques. Measurement quality for series production must also address sensor-to-sensor variability, where variations in component characteristics within their tolerances—such as resistance or capacitance, coating thickness, etc.—can cause significant differences in output between sensors for the same soil sample.

2.4. Permittivity-Based Measurement Techniques

2.4.1. Overview

Measuring soil variables, such as Θ_v, is more difficult than measuring counterparts in the atmosphere, like air relative humidity, because air is a gaseous phase homogenized by convection. The only direct method to obtain Θ_v is by weighing and oven-drying soil samples, which is expensive and nearly impossible to automate [22].

The most suitable indirect method for in situ sensors, especially for our goal of autonomous wireless sensors, is based on another intrinsic soil variable: its dielectric permittivity. Permittivity measures the response strength of medium electric dipoles to the electric field induced by an instrument between its electrodes. The normalized or relative quantity, $\boldsymbol{\varepsilon_r}$ (using the vacuum permittivity $\varepsilon_0 = 8.854$ pF·m^{-1} as a reference), is $\boldsymbol{\varepsilon_r} = 80$ for liquid water at 20 °C due to its strong molecular dipoles, whereas it is about $\boldsymbol{\varepsilon_r} = 4$ for solid grains in soil, and is $\boldsymbol{\varepsilon_r} = 1$ for air (confounded with that of vacuum). Hence, soil $\boldsymbol{\varepsilon_r}$ is strongly influenced by the volume of water present in the soil. However, because of the tortuous distribution of these different phases in soil, Θ_v cannot be directly obtained from the knowledge of soil permittivity and the permittivity of its different phases. Furthermore, the presence of ions in pore water and on grain surfaces, apart from their direct contribution to soil bulk conductivity σ, can act as dipoles around the soil's non-conductive grains [23]. Measurements with samples in the laboratory show that this polarization effect depends on the frequency, f, of the alternating electric excitation applied to the medium [24–27]. Relaxation of ionic polarization occurs below 10 MHz, with the limit decreasing as the amount of clay increases but increasing with water content and salinity. The ionic contribution to $\boldsymbol{\varepsilon_r}$ vanishes at the end of the relaxation. Moreover, the dipolar relaxation represents a dissipation mechanism of the electric energy in the medium, hence contributing to σ, along with the ionic conduction. It equally disappears at the end of the relaxation. On the other hand, literature abounds with physical modeling of these phenomena in soils and rocks, as well as relations for converting $\boldsymbol{\varepsilon_r}$ into Θ_V, ranging from extended Archie's laws [28] to Topp's empirical correlation [29] and the effective medium approach [23]. Interestingly, the mathematical processing of electromagnetic equations for soil to derive physical relations considers the variables $\boldsymbol{\varepsilon_r}$ and σ as the two parts of a complex permittivity variable, $\boldsymbol{\varepsilon_r}$, despite different origins [28].

No instrument—except maybe the one developed by M. Hilhorst [30]—measures the complex quantity $\boldsymbol{\varepsilon}_r$, that is, measures $\boldsymbol{\varepsilon_r}$ and σ simultaneously with the same electrodes and circuit at the same frequency. Recent sensors that provide σ operate with a different instrument than the one used to measure Θ_V, sometimes sharing the same electrodes [31]. Moreover, few sensors can directly retrieve $\boldsymbol{\varepsilon_r}$, making the above theoretical relations useless for most of them. Instead, empirical relations between sensor output and Θ_V obtained with soil samples are used. However, to have a reliable and specific assessment of instrument performance, and because soils cannot be considered standards for this purpose, sensors should be calibrated against homogeneous fluids of known permittivity [32,33]. The use of fluids with controlled salinity should complete instrument characterization to assess sensitivity to σ independently of the contribution of salinity to soil $\boldsymbol{\varepsilon_r}$. Thus, in addition to the Θ_v-reading curve obtained with soil, a permittivity-reading curve must be provided—the so-called two-step approach. Unfortunately, this is rarely done.

Permittivity-based instruments produce electromagnetic fields in the medium under study, propagating along a direction z, which corresponds to the axis of the sensor electrodes or guide. These fields, which are solutions of Maxwell's electromagnetic equations in a dielectric medium (as introduced in the classical textbook [34]), present the general form:

$$A[\varepsilon_r]\, ph\left[\frac{z\,\mathrm{Re}(\sqrt{\varepsilon_r})}{c} - t\right], \quad (1)$$

where A is the field amplitude and ph is the field phase with dependence expressed in time. The quantity c is the velocity of electromagnetic waves in a vacuum (c is approximately 0.30 Gm·s^{-1}) and $\mathrm{Re}(X)$ is the real part of the complex quantity X.

Both A and ph depend on ε_r. The choice between A and ph to deduce Θ_v defines the two large families of permittivity-based sensors.

2.4.2. Phase-Based Family of Sensors

In the case of the phase-based family, the objective of any measurement technique is to determine the time or phase delay for a generated wave to travel forth and back along the waveguide, knowing the travel length. The expression $\mathrm{Re}(\sqrt{\varepsilon_r})$ is approximated to $\sqrt{\varepsilon_r}$ for most of the soils, which allows an analytical relationship between instrument output and ε_r. The variable σ plays a role in wave attenuation, which can make determining the travel time difficult. The guide can be straight rods in the soil, with the wave being partly reflected at the free end or forming a loop connected at both ends to the electronic circuit. A very common instrument in this category is the time domain reflectometry (TDR) or time domain transmission (TDT) sensor, which generates step-like transverse electromagnetic waves and records the return signal at the circuit input to determine the travel time [29]. ε_r is determined by setting the variation of phase in Equation (1) to zero between the start and the end of wave propagation along the guide, with z being the travel length. For $z = 60$ cm, the time is about 2 ns when the guide is in the air and 18 ns is in water. The instrument requires high-speed electronics to generate and record the signal, as well as an algorithm to determine the time of the return signal, despite its deformation by frequency dispersion and amplitude attenuation. This makes it expensive and energy-consuming. Campbell Scientific's TDR SoilVue [35,36] is more compact than previous sensors and can measure various soil variables, each with a specific circuit, at different depths in the soil. The instrument costs USD 1700 w/o VAT for the six-depth model and requires 45 J for one measurement, as well as 18 mW of power in quiescent mode. It does not include the external data logger needed to supply power and to store and transfer its digital output.

A compact and low-cost version of TDRs, called reflectometers or transmission line oscillators, consists of an electronic oscillator that triggers an impulse once it receives the return wave [37,38]. This generates a cyclic output with a period related to the wave travel time. Campbell Scientific offers some of these, such as the CS650 [38]. However, the output is not as directly related to travel time as in traditional TDRs. It also includes a dead time before the generation of a new pulse, which is sensitive to electronic temperature. the attenuation of the return signal due to salinity increases the travel time at the same permittivity resulting in an apparently higher permittivity (as observed with the CS650 [38] and similar probes such as the CS616). This makes it impossible to analytically relate instrument output to medium permittivity as with true TDR. Despite its lower cost, Campbell Scientific did not retain the technique for its latest product. FieldScout TDR 100 (Spectrum Technologies Inc., Aurora, IL, USA), TRIME-PICO64 probe (IMKO, DE) [39], STM100 (Truebner GmbH, Neustadt an der Weinstraße, Germany) [40], and the temperature–moisture sensor (TOMST s.r.o., Praha, Czech Republic) [41] use this measurement technique and should experience the same problem.

Moreover, a coating or protective plastic around the sensor probe, like the two later ones—made from a PCB—introduces a low-permittivity medium in series with the medium under study. Depending on the geometric importance of the layer and, therefore, electrode geometry, its contribution to instrument output increases with medium permittivity or moisture in the case of soil. As a consequence, the instrument becomes less sensitive to variations in medium moisture, as observed with the STM100 [40]. This bias is encountered in any sensor using a low-permittivity layer to protect its probe, independent of its

measurement technique, as shown in the case of the EnviroSCAN instrument by Senteck; Kelleners et al. [42].

2.4.3. Amplitude or Capacitance-Based Family of Sensors

The second group of sensors relies on the amplitude of the dielectric response in Equation (1). These sensors usually operate at frequencies close to or lower than 100 MHz, i.e., with a wavelength in a vacuum larger than 3 m. Given an electrode length smaller than 10 cm, the propagation effect is assumed negligible. The sensor electrodes embedded in the soil are modeled as capacitors, of which admittance is $Y = G + \mathbf{j}\, C\, 2\pi\, f$ with C denoting capacitance and G denoting conductance, in parallel. Sensors of this family are labeled capacitance sensors. An alternating excitation v_{exc} is applied between electrodes resulting in a current i_x through the capacitor. Admittance, Y, and the apparent permittivity of the medium, $\boldsymbol{\varepsilon_r}$, are defined according to the generalized Ohm's law, as follows:

$$i_x = (G + \mathbf{j}\, C\, 2\pi\, f)\, v_{exc} = \left(\frac{\sigma}{2\pi\, f} + \mathbf{j}\, \varepsilon_0\, \boldsymbol{\varepsilon_r}\right) g\, 2\pi\, f\, v_{exc}\,, \tag{2}$$

where g is a factor depending only on electrode geometry.

For this type of sensor, a third step of characterization could be achieved by using reference resistors and capacitors at the circuit input in place of electrodes. In practice, at frequencies (f) above 10 MHz, it is very difficult to build an electric circuit to directly exploit Equation (2) due to low phase resolution and parasitic impedances introduced by the instrument [30,43]. Instead, indirect electronic methods are used, with the output limited to a single signal. Instruments of the company Sentek Sensor Technologies Ltd.,Stepney, Australia, are based on an inductor–capacitor oscillator, of which the resonant frequency is the instrument output [42]. The capacitor comprises the electrodes in the medium, as well as the parasitic capacitance and inductance from the instrument circuit. Kelleners et al. suggested an equivalent circuit that takes into account probe conductance, G, due to medium conductivity, as well as the capacitance of an access tube. It allows us to analytically predict their influence on the output, chiefly reducing its sensitivity to medium real permittivity, i.e., moisture.

Regarding sensors from Delta-T Devices and Stevens Water Monitoring Systems, the probes form the end of a coaxial line where a reflected electromagnetic sinusoidal wave propagates along the line [25,44]. Instrument modeling for these sensors is more complex, necessitating empirical relationships.

The measuring circuits of many other sensors provide a periodic square excitation for charging and discharging the probe, operating in the time domain rather than the frequency domain (where $\mathbf{j}\, 2\pi\, f$ in Equation (2) becomes the time derivative of voltage). This is the case for sensors commercialized by the Meter Group (ex-Decagon, Pullman, WA, USA) [45], as well as more recent ones such as the single depth (SD) device from Sensoterra B.V., The Netherlands [46] and the low-cost blade-shaped probes available on the internet [21,47,48]. The characteristic time of the exponential charging or discharging of a capacitor is determined by its capacitance and the resistance in series with the square wave generator. Usually, the resistance is fixed in the circuit and the capacitance is partly that of the probe, although in the case of the Sensoterra device, it seems the opposite. The challenge is to provide a constant output from a varying voltage at the capacitor ends, which depends on the probe capacitance. Different methods are employed, such as measuring the charging time up to a threshold voltage (devices from Sensoterra BV, Houten, The Netherlands), using the RMS average after imposing a threshold voltage (Meter Group's sensors), or holding the maximum voltage over the excitation interval. None of these methods allow for analytical modeling of the circuit, which would permit the study of output sensitivity to salinity, electronic temperature, or the tolerance of instrument components. A study of the electronic circuit of the probe made from PCB shows the out-of-specification operation of the timer used as an oscillator at a frequency of 1.5 MHz, which increases sensor-to-sensor variability [47]. Actually, the data sheet provided on the internet

page by the manufacturer DFRobot indicates that the probe is intended to determine between three states of soil, dry, wet, or saturated [21]. When tested with soil samples in the laboratory, Sensoterra devices present sensor-to-sensor variability, sensitivity to σ, and a sensitivity to soil moisture diminishing when Θ_v increases above 20%.

Another point to examine for measurement quality is the volume of soil sampled by the probe. The volume is defined by the square of the electric field amplitude in the medium [49]. The stronger the squared amplitude in a soil part, the larger the weight of this part in the moisture average determined by the instrument (hence, the importance of probe geometry). In the case of planar electrodes on the same surface, such as along a cylinder (EnviroSCAN of Sentek tech. Ltd., Stepney, Autstralia, PR2/4 or PR2/6 of Delta-T devices, the multi-depth sensor of Sensoterra, etc.) or on the PCB surface, the electric field is concentrated close to the surface between electrodes. The sampled volume is small and may be affected by the air gap between the soil and probe surface or by any perturbation of soil during insertion. A better probe geometry to increase the volume consists of two parallel cylindrical rods, like the single-depth device of Sensoterra, as the field extends around and between the rods. However, when the rods are too far apart from each other—more than four rod diameters—their extension perpendicular to the rods is mainly controlled by their diameter [49]. The use of thin rods, like those in the CS635 probe of Campbell Scientific, allows for easy insertion into the soil but at the expense of representativeness. The electrodes of the TDR SoilVue form threads around a 60 mm cylinder, which are the usual thin rods of older TDR designs. This geometry further reduces the soil sampling volume, as only the rod part in contact with the soil contributes.

Electrodes of in situ sensors must be inserted into soils and, as a consequence, soil invasiveness is unavoidable. It is all the more disturbing as various probes must be placed at different depths along a profile. Moreover, very often, electrodes are directly attached to the measuring circuit to avoid the parasitic contribution of a lead, which increases probe volume. Two techniques have prevailed. In the case of independent planar probes intended for one depth (fork or PCB), a trench is dug to place probes horizontally in the soil through the trench wall. Probes are connected to an above-ground data logger in a modular approach. The alternative is to insert in the soil a cylinder with electrodes along it after boring a hole at the cylinder diameter. The cylinder diameter is large enough to include measuring circuits, usually higher than 30 mm. Because the process is less labor-consuming and disturbing, it is more and more favored, as shown with the latest products from Campbell Sc., Logan, UT, USA (TDR SoilVue) and Meter group (TEROS 54). TDR SoilVue is in the form of a 60 mm diameter screw that is inserted into the soil by rotating it with a special tool. Its diameter accommodates all the electronics inside, but this makes it invasive. Prior to probe insertion, the same volume of soil as the probe must be removed with an auger.

Two recent sensors, the TEROS 54 sensor from Meter Group and the single-depth device from Sensoterra, offer notable features in terms of sampling volume and field installation, despite their electronic drawbacks. The former consists of a 70-cm-long and 2-cm-wide inner shaft equipped with four wings, resulting in an overall diameter of 6 cm. It requires a 2 cm hole and a slide hammer for installation. Soils are probed over four 7-cm-high horizons at depths from 15 to 60 cm. The wings, which form part of the electrodes, help to increase the sampled volume between them. There is no information about the location of the measuring circuits. If they are located in the 11 cm-wide head at the top of the cylinder rather than close to the electrodes inside the shaft, lead inductance and interference between electrodes at different depths due to close lead contact could render the instrument unsuitable for accurately measuring real permittivity and, therefore, water content, as explained in the Section 3.1. Moreover, the device requires a data logger for operations, data transfer, and power supply. The Sensoterra sensor is an integrated device, from the LoRa antenna to the electrodes in the soil, designed to be compact and easy to install. The probe consists of two parallel cylinders, each 6 mm in diameter and approximately 20 mm apart, with the 35-mm-long bottom forming the probe electrodes.

This geometry increases the sampled volume while remaining compact. The length of the probe determines the depth of the soil horizon to be sampled, ranging from 15 to 90 cm. All electronics are housed in an 8-cm-diameter casing at the top of the rods and above ground, which means a long lead to the electrodes. There is no information about how to account for its contribution to signal processing [46]. Moreover, the device's geometry, with a large housing at the surface above the electrodes and a flange between the rods in the soil, may disturb rainfall and water infiltration. The soil at the electrode level may not be representative of the soil away from the probe.

3. Materials and Methods

A Multi-Variable Multi-Horizon Wireless Sensor

The sensor described here is the result of over ten years of development and trials, involving successive generations of prototypes [20]. Its design is tailored to meet the goals of our project, HYMENET, which stands for Hydro Measurement Network—a network of in-situ sensors for hydrological measurement in soils. Initially supported by the program 'Critex'—Challenging equipment for the temporal and spatial exploration of the critical zone at the catchment scale—from 2014 to 2020, it is currently backed by another significant research infrastructure project, EquipEx+ funded by ANR, named TERRA FORMA (2021–2029). The project's aim is to fundamentally transform the paradigm in the observation strategy of anthropized natural systems.

Two recent articles have detailed the characteristics and experiences gained with the latest generation of our single-depth device in two key aspects. Firstly, the device's autonomy in terms of operation, communication, and energy for long-term monitoring [20]. Since 2018, the LoRaWAN radio mode has been adopted for our devices, as it meets the requirements for long-range, low-consumption, real-time data throughput. Secondly, the measurement component utilizes a self-balanced Wheatstone bridge to directly determine the pair of soil variables, ε_r and σ [33]. It allows for complete modeling of the instrument using the electric circuit theory. The model enables the determination of coefficients for the conversion chain of output voltages into ε_r and σ, and to study the influences of external factors and specification tolerance. Calibrations with reference components and liquids complete the theoretical work to increase accuracy.

The latest generation prototypes have laid the foundation for a demonstrator that addresses the challenges and specifications outlined in the introduction, namely monitoring accurate profiles of soil variables, achieving autonomy, and reducing costs (see Figures 1 and 2). The choices made for this purpose may entail certain risks or drawbacks. Efforts have been made to mitigate these risks or find solutions to overcome them.

- To reduce costs and enhance compactness, an integrated design similar to that of Sensoterra for its single-depth device is adopted. All electronic components, measurement circuits, acquisition systems, the micro-controller, real-time clock, LoRa transceiver, and memory, are housed in an IP66 enclosure measuring $12 \times 12 \times 5.5$ cm^3 dimensions with a crystal lid. This lid allows for rapid checks and houses a solar cell. Integration is further enhanced by mounting all electronics on a single PCB. The enclosure is positioned above ground, close to the probes, and is supported by four legs with points that firmly anchor it into the soil. The same electronics serve multiple probes in the soil for multi-horizon, multivariable monitoring. The probes are modular, as they are detachable, allowing for a choice between different configurations (details provided further down).

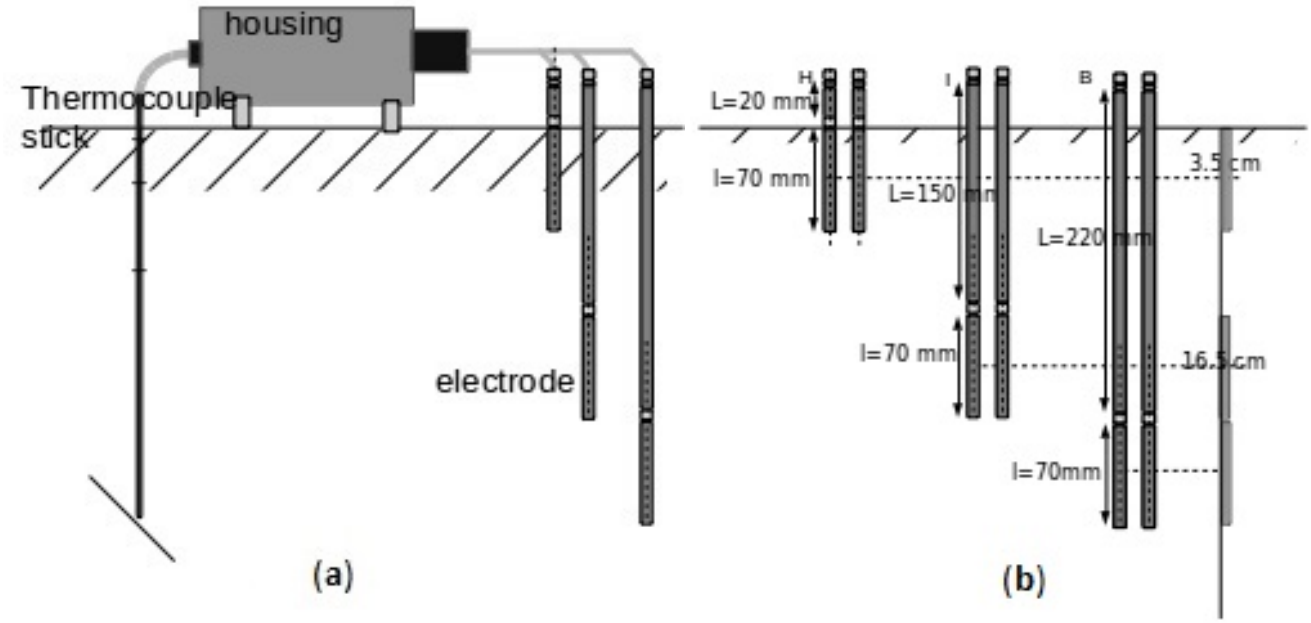

Figure 1. Schematic views of the sensor with probes in soil to monitor the moisture and salinity profile on one side, and the temperature gradient profile on the other side: (**a**) side view. (**b**) The three probes monitor soil moisture at three horizons (labeled 'H', 'I', and 'B', from the shallowest to the deepest). The sensing part is the 7-cm-long electrodes at the probe's bottom.

Figure 2. Photo of the new demonstrator operating in the field. The three moisture/salinity probes are visible in the left hand, each sensing a different soil horizon at depths ranging from the surface to 30 cm. The housing contains a Li–ion battery in parallel with a solar cell fixed in the lid. The antenna on the right hand transmits data in real time via LoRaWAN. The thermocouple stick was not used.

- Data retrieval for autonomy: The task is carried out only through LoRaWAN in real time (no manual retrieval from a memory by a USB cable or key). The sensor is designed to remain at an isolated site with interventions limited to troubleshooting. There is a risk of losing some measurement points, but this is mitigated by using a high-quality antenna (potentially positioned above the housing on a mast with a cable), ensuring a clear line of sight to LoRaWAN gateways, selecting a large spreading factor (SF), or increasing the measurement frequency. However, the last two solutions increase device consumption and are considered last-resort options. As the last 2000 points are temporarily stored, one method involves re-sending any missing points upon request via a LoRaWAN downlink. It is possible to automatize the method and limit the retrieval only to points of interest.
- Data time stamp: This is fixed by servers of the LoRa network once the message is received from a gateway. The server time is synchronized with the universal clock time whereas time from the device is affected by quartz drift (about 1 s per day for common quartz, or 6 min per year, or a relative uncertainty of $\pm 10^{-5}$). The risk of the procedure is the potential time latency from the gateway to the server for some messages (1 to 50 or 100). On the other hand, the time stamp is controlled using the time difference between two successive messages, which should remain close to the measurement time step, Δt, of the device within the uncertainty defined by device drift, i.e., $\delta \Delta t \sim \pm 10^{-5} \Delta t$. The whole procedure avoids the use of a GPS module inside the sensors.
- Energy consumption: This depends on the power need and duration of activation of each successive operation during the active phase, which involves the measurement and transfer via LoRaWAN. The self-balanced bridge—due to its high-phase resolution—requires significant power (initially, 3.3 W). The use of passive components instead of some active or low-consuming new ones reduces the power to 2.2 W. With an activation time limited to 150 ms for four channels, the consumption per point is equivalent to that of LoRaWAN communication when working with SF 11 or 12. Moreover, consumption is proportional to measurement frequency. By sending a request with a downlink, the frequency can be reduced when meteorological conditions indicate no need for high temporal resolution. The procedure could be automatized and coupled with information from a meteorological station.
- Energy autonomy: The choice between different sources of electric energy is viable as long as their voltage remains between 3 and 5 V and their dimensions fit within the free space of the enclosure. One option could be alkaline batteries arranged in a 3S2P configuration (three in series, two in parallel). These are low-cost but have limited capacity and are sensitive to cold temperatures. A better alternative might be Li-ion batteries coupled with a 5×10 cm^2-area low-cost amorphous Si cell. The capacity of the Li-ion battery is chosen to be just large enough to smooth out the Si-cell's contribution over a year. Depending on the site, this could range from a single cylindrical cell (1S1P) to up to three in parallel 1S3P.

As a result of the separation between measuring circuits and sensing parts, a modular and low-cost approach has been used for the probes.

3.1. Soil Moisture and Salinity Profile

The measurement principle is based on Equation (2) [33]. An excitation of v_{exc} at $f = 24$ MHz is applied between the electrode ends. However, the resulting complex current i_x is not directly measured. Its two components are automatically balanced in less than 10 ms by currents from the bridge's capacitance and conductance branches. Each current linearly depends on a direct voltage, V_C or V_G, built by a feedback loop until i_x is exactly balanced, which constitutes the output. The bridge presents a high-phase resolution, down to 0.0005 rad, to distinguish the capacitance C_x and the conductance G_x at its input. Assuming that both represent the two parts of electrode admittance, the bridge output verifies the following:

$$\begin{cases} \varepsilon_r = C_x/(\varepsilon_0\, g) = C_{eq}\, V_C/(\varepsilon_0\, g)\,, \\ \sigma = G_x/g = G_{eq}\, V_G/g\,, \end{cases} \tag{3}$$

Parameters C_{eq} and G_{eq} are bridge sensitivity factors fixed by key circuit components. The geometry factor, g, is determined analytically in the case of electrodes made of two parallel cylinders [49].

The bridge phase resolution is the first condition to allow the separation of $\boldsymbol{\varepsilon_r}$ from σ at the probe level. The balanced bridge is analytically modeled. Presently, ranges are fixed by construction for $\boldsymbol{\varepsilon_r}$ between those of air and water, and from 0 to $\sigma = 175$ mS·m^{-1}. These ranges can be extended with some modifications to the bridge circuit.

The bridge circuit contains its own power regulator and A/D converter module to be isolated and switched off once a measurement is achieved, despite being on the same printed board as other circuits.

The points to consider for accuracy, cost, and consumption of the whole instrument are as follows:

- The values of components present some dispersion within their tolerances, especially for active ones, which is detrimental to bridge offset and phase resolution. Consequently, bridge branches present phase errors that produce interferences between them. Moreover, these biases vary from one bridge to another. A procedure has been defined to solve this problem. For each measurement point, the offset is automatically acquired and then subtracted from raw voltages before sending data. Each branch has a phase shifter with a potentiometer to correct its phase error. The control is achieved using a reference input or channel, comprising a selectable high-quality capacitor and resistor (with 1 and 0.1% tolerance, respectively, and thermal drift of ± 30 ppm·°C^{-1}), connected to the bridge like a probe. Potentiometers are adjusted to reach specific output values for each component. The control is simple enough to be carried out by the end user.
- The reference channel adds negligible cost while enabling the first step of calibration and control at the bridge circuit level. The values of linear coefficients C_{eq} and G_{eq} in Equation (3) are precisely determined and should be close to the values given by circuit modeling within uncertainty intervals. Along with an onboard numerical thermometer, the channel allows for the study of bridge sensitivity to electronic temperature T_{elc} [33]. It verifies that the high-quality resistors and capacitors chosen for key components of the instrument produce an overall drift of about ± 200 ppm·°C^{-1}, which amounts to ± 0.8% for a variation of $\delta T_{elc} \sim 40$ °C. The use of liquids instead, as described in this work [50], produces larger uncertainty since the dependence of permittivity on temperature introduces an additional error source. The reference channel even provides a means to correct residual drift. During field operation, the reference channel permits checking the functioning of the bridge circuit in real time, independently of any probe troubles.
- High-phase resolution of the bridge at $f = 24$ MHz (potentially 50 MHz) requires costly large-band components. Some new components have reduced both cost and consumption while maintaining bridge performance. Moreover, the same circuit is shared by all probes in the soil, presently three, potentially four, thanks to relays that successively connect each of them to the bridge for measurement. Relative to other systems described in the introduction, which require different modules to achieve the same result (a completely autonomous device for profile monitoring), the overall cost is actually lower with this integral approach.
- One probe represents a soil horizon between two depths. It consists of a pair of standard stainless steel tubes and, at their bottom end, a stainless steel rod acting as an electrode. The material provides mechanical strength and resistance to corrosion while ensuring direct electric contact with the soil. Both metallic parts are attached using a plastic headless screw with a low coefficient of thermal expansion. The lead to the bridge through the tube is electrically connected to the rod by tightening the plastic

screw at the rod's top end. The connection remains secure even in cold conditions, as confirmed during assembly. Probes are detachable from the circuit housing using IP66-rated connectors, allowing for easy replacement in case of issues. For each input or channel of the circuit, a choice between probes or depths is possible. However, due to standardization, the number of available depths must remain limited to two per channel.

- The probe geometry, consisting of a pair of vertical parallel tubes and rods, is very similar to those of SD Sensoterra. Both cylinders are 20 mm apart and have tube and rod diameters of 8 mm. The diameter is slightly larger than that of SD Sensoterra to increase the sampled volume [49], while still facilitating installation and limiting invasiveness. The rods, also known as electrodes, are either 7 cm or 10 cm long. The probes cover different soil horizons to assess soil water content over the profile and detail its vertical distribution. Figure 1 shows the set of probes used in the trial presented in this article. Note that, due to the modular approach, a different geometry can be chosen for the probe, such as a single cylinder with two electrodes along it, provided it is compatible with the housing connector and bridge input.
- Rainfall above ground and infiltration below ground should remain free from obstacles. There is no flange during operation between the vertical cylinders in the soil, and the electronic housing above ground is 10 cm away from the cylinder tops (see the photo in Figure 2). Each cylinder top is fitted with a cable gland of the same diameter. The lead between the gland and housing is protected by a 6 mm sheath. Probes and housing must be firmly secured to ensure measurement quality. Wires are tightly fixed to the housing with a connector. Trials conducted for at least a year show little displacement in the soil (change of distance between cylinders or upward movements), even for the shortest cylinders. To firmly anchor the probe in the soil in such cases, a rod could be fixed at the electrode bottom with a headless plastic screw, similar to the top.
- The drawback of the instrument design is that the distance between the measuring circuit and electrodes increases with depth. The lead introduces an inductance in series with electrode admittance to be determined. The inductance produces a cross-interference on instrument output between electrode capacitance C and conductance G, independently of bridge performance. However, the impact is accurately modeled. Moreover, the inductance is offset by a capacitor at the bridge input in series with the lead. The capacitor value is determined by instrument modeling and calibration with liquids. As it depends only on probe materials and dimensions, the same capacitance is used for all identical probes in a series production, within the capacitance tolerance of the component (i.e., 1%). The lead length introduces signal attenuation, about 20% in the case of a 50 cm depth. As for the inductance, the effect is assessed once, and correction is applied to all identical probes. This is the reason to limit the choices of probe lengths and, therefore, depths.
- Another drawback is the potential influence of the external environment on the lead signal outside the sensing part, chiefly soil along tubes between electrodes and the soil surface. The lead must be thin, typically 250 µm, and centered in the tube to make it negligible, as detailed in reference [51].
- This impact is distinct from the fringe effect of a capacitor due to the limited length of its electrodes. The effect modifies the value of the factor g in Equation (2). The correction depends on the ratio of the cylinder length to their distance, which is 1.20 for a probe with a length of 70 mm. This has been thoroughly studied through simulations and laboratory calibrations, as described in reference [51].
- Why are electrodes for different depths not all assembled on the same cylinders? It is mechanically difficult to assemble different tubes with many wires inside while maintaining an 8 mm diameter. The labor cost is higher than using three independent probes. This design does not offer a modular approach. If a problem occurs in one part of the probe, the entire instrument can become nonfunctional. Moreover, another

important reason is the occurrence of cross-interferences between the leads of the different electrodes due to their close contact inside the tubes. This phenomenon can be reproduced with only two pairs of wires, each connected at one end to a resistor and/or capacitor in parallel and the other end to the measuring circuit, mimicking two probes in close contact. The output for one pair is influenced by the component in the other pair, even if its wires are completely disconnected from the bridge circuit. Due to operating at a high frequency, a capacitive influence and a mutual inductive effect exist between the two pairs of wires, which are more pronounced when the wires are close together. This was previously accounted for using a semi-empirical model with some approximations [52]. However, that model applied to leads far apart in a 50 mm cylinder, resulting in a small correction. With independent probes, cross-correlation is reduced to less than 1%, which can be verified by disconnecting one probe and—at the same time—measuring the variations in output for the other two (see Figure 3).

- Installation must ensure that the two cylinders of a probe remain at the same distance and parallel. A thick block with three pairs of parallel holes drilled across it, placed firmly on the soil, guides a metallic rod to bore the emplacement of each cylinder for three probes. A flange can be temporarily used between cylinders to hold them in place while inserting the probe into the soil after preparation. In the case of loose and humid soil, a probe with a removable flange can be directly inserted.

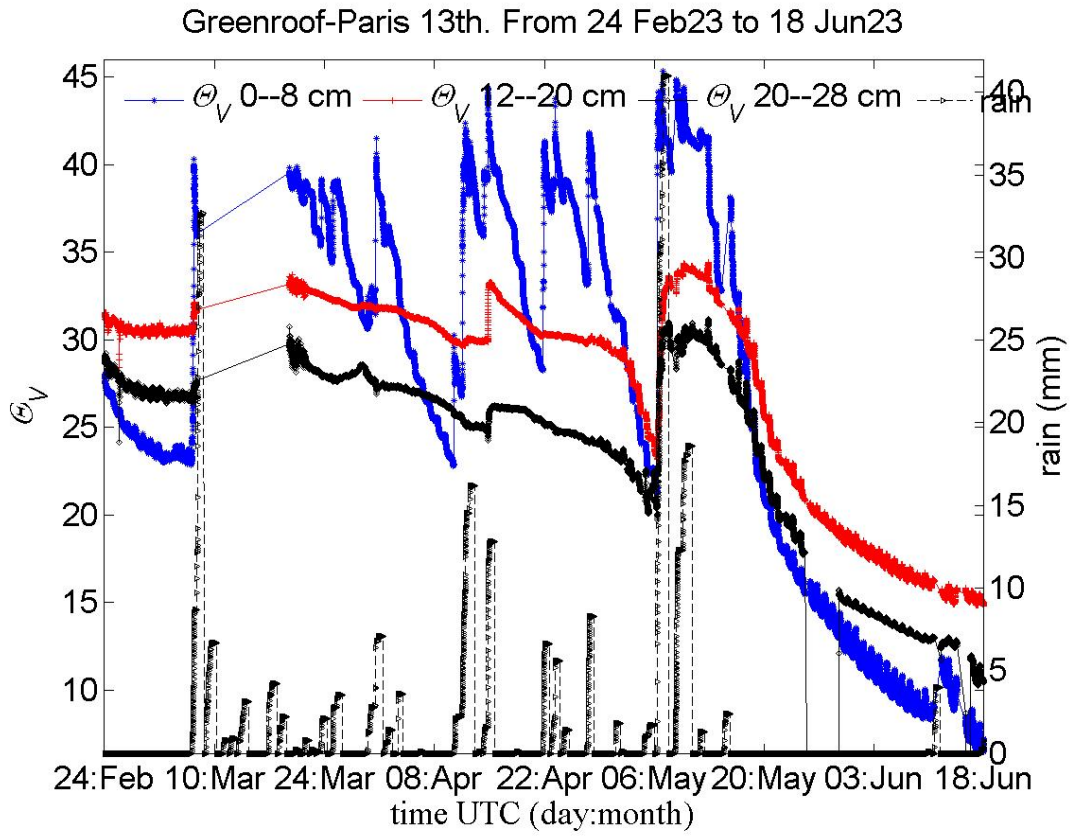

Figure 3. Variation of soil moisture from 24 February to 18 June 2023, as measured by the device over the three horizons covered by sensor probes (see view (b) of Figure 1), taking into account fringing effects. Precipitations during the period, from an on-site rain gauge, are also reported.

Determining soil permittivity and bulk conductivity at $f = 24$ MHz allows for the testing and use of conversion formulas of ε_r and σ into Θ_v and salinity, as discussed in the introduction. This should limit the need for extensive sensor characterization with soil samples, allowing for reliance on one formula.

3.2. Soil Temperature Profile

Apart from the broader interest in monitoring the soil temperature profile mentioned in the introduction, it also allows for the study of any correlation between variations in soil conductivity, or even moisture, and temperature changes at similar depths.

The measurement principle is based on the acquisition of the voltage difference between two junctions of two thermocouples at different heights in a probe. The voltage is proportional to the difference in temperature ΔT between the junctions. The coefficient is well referenced for each type of thermocouple, even the coefficient drift with the absolute temperature, which introduces some non-linearity [53]. Therefore, no calibration is required to obtain a resolution for ΔT lower than 0.01 °C, at the difference of absolute thermometers. An absolute thermometer is still necessary for an accurate value of the thermocouple coefficient, but at a precision of about 0.1 °C, without the need for calibration. One of the difficulties involves acquiring low voltages due to the typical thermocouple sensitivity of 50 µV/°C (40 µV/°C for type J or T thermocouples, 60 µV/°C for type E), and small temperature differences in soil, which are often lower than 10 °C or less than a few °C.

In our latest instrument design, thermocouple voltages are measured with an integrated module using a 24-bit A/D converter, the LTC2986 from Analog Devices, US—formerly Linear Technology. The instrument has a gain error of less than 1%, and an offset smaller than 1 µV. Despite its complexity, limited resolution, and cost, it is chosen because it is readily available with a resolution close to 0.01 °C. Other recent 24-bit A/D converters feature higher resolutions at lower costs but require a procedure to be designed and tested in order to correct their offset and reduce uncertainty in gain, both of which vary from one component to another. The LTC2986 also measures the absolute temperature from various types of thermometers without the need for calibration. Like the bridge circuit, the temperature-measuring circuit on the device's printed board is independent, with its own power regulator that can be switched off when the instrument is idle.

The circuit inputs accommodate the connection of five thermocouples and a resistive thermometer, such as a Pt1000 resistor. In our design, the LTC2986 is configured to measure the Pt1000 resistance and convert it into temperature, with the value sent in the LoRa message. The five thermocouple voltages—four corresponding to voltage differences between adjacent thermocouples and the last one to the voltage between two wires of a thermocouple—are transferred without conversion. The input settings allow for the choice of all types of thermocouples, their number (up to five), and their usage mode (differential or absolute). Thus, this flexibility permits the connection of heat flux plates, such as the HFP01 commercialized by Hukseflux Thermal Sensors B.V., to determine soil heat flux across the plate.

The probe used in the trial is a thermocouple profile stick (manufactured by Prosensor SA, Amanvillers, France.) It is made of a thin stainless steel tube with an outer diameter of 5 mm, a wall thickness of about 0.5 mm, and a length of 480 mm. Inside, five type T thermocouples (Cu/NiCu) class 1 are placed in a geometric progression along the tube. At the bottom of the stick, the first thermocouple with a Pt1000 thermometer is placed; the next thermocouple is located 240 mm above the first, followed by another at 360 mm from the bottom, the penultimate at 420 mm, and the last one at 450 mm. The latter is positioned 30 mm from the top of the steel tube, from which the thermometer wires emerge. The probe is inserted into the soil so that the uppermost junction is 1 cm from the surface. Each wire of a thermocouple is made from a 0.2 mm single strand insulated by a polytetrafluoroethylene sheath with an outer diameter of 0.5 mm. Outside the tube, the wires are protected by a white heat-shrinkable sheath. Part of the stick above ground is also insulated by a heat-shrinkable film to reduce thermal exchange with the outside environment.

The stick's small diameter facilitates easy insertion into the soil with minimal disturbance. It is designed to continuously monitor the vertical profile of soil temperature. Using a soil thermal conductivity model, such as Johansen's correlation [54], and soil water

saturation data obtained from the device, vertical fluxes are determined. Otherwise, the inverse resolution of the heat diffusivity equation provides soil diffusivity estimates.

What about the potential drawbacks of the design? Does the temperature vertical profile inside the stick match that of the adjacent soil? Is there a risk of the steel wall creating a thermal shortcut?

Steel conductivity is about 20 $W \cdot (K \cdot m)^{-1}$, which is much lower than that of copper. Nevertheless, the primary reason for low heat diffusion along the probe is the thin metallic wall. The characteristic time for the steel shell to reach thermal equilibrium with the surrounding soil is short, about 0.06 s. Moreover, the ratio of this time to the time for heat to diffuse along a height, z, of the probe is fixed by the square of the ratio of the wall thickness to z. Therefore, the time to reach equilibrium with soil temperature is much shorter than the time for diffusion along the probe for z larger than a few millimeters. To reduce any risk of potential departure due to heat flux along the steel wall from an external source, such as stick-head heating from the sun, insulation like a heat-retractable white tube is added around the head and wires above ground.

Thus, the thermal gradient in soil, resulting from solar input and cooling during the night, is rapidly the same along the probe.

Uncertainty in temperature ΔT and depth difference between junctions are roughly assessed as follows:

$$\begin{cases} \delta\Delta T = \pm 0.02\,\mathrm{K}\,, \\ \delta\Delta z = \pm 1\,\mathrm{mm}\,. \end{cases} \tag{4}$$

4. Results and Discussion

Data presented in this section were recorded during a trial with a prototype to test the optimized bridge circuit, using new components, with the set of probes shown in view(b) of Figure 1.

The trial took place during spring 2023 on a green roof at the top of the laboratory building. It is located in the 13th Paris district at a latitude of 48.828 N and a longitude of 2.3806 E.

The soil thickness is about 50 cm over a square area of 15 m in length. Soil mineralogy, obtained from X-ray diffraction, is mainly composed of quartz (more than 83%, with the rest being feldspar and clay (up to 8%). Granulometry obtained from sieves (with the lowest mesh at 63 µm) shows a maximum grain size between 125 and 90 µm. The soil can be classified as silty/loamy sand. In the top 5 cm, the soil has a dry bulk density of about 1.0 $g \cdot cm^{-3}$, which means a porosity of 63%. From 10 to 15 cm, the density is about 1.09 $g \cdot cm^{-3}$ (a porosity of 59%); below 15 cm, the density is about 1.25 $g \cdot cm^{-3}$ (a porosity of 53%).

4.1. Soil Moisture and Water Balance

Figure 3 shows soil water contents as determined by the device during the trial over three soil horizons, along with cumulative precipitations during rain events. We use Topp's correlation to convert the real permittivity ε_r into soil moisture Θ_v. This correlation is established with TDR sensors [29]. The direct determination of the water content in a soil sample near the surface indicates a moisture level of 33%, which is within 2% agreement with the sensor measurement at the surface horizon during the same time interval. This correlation remains an approximation, but it is considered sufficient for this trial to test new designs and some sensor capabilities.

The probe design allows for monitoring soil moisture at three horizons (labeled 'H', 'I', and 'B'). It does not cover the horizon between 8 and 12 cm depths, even accounting for fringing effects, which extend the sampled soil volume up to 1 cm from each end of the electrodes. To obtain a complete water balance from the soil surface to the bottom end of the deepest electrodes, moisture over the gap is calculated by interpolating the moisture measured at the two adjacent horizons. This approach is not valid during a rainfall event when an infiltration front progresses downwards in the soil.

Measurements started at the end of winter 2023, coinciding with the last days of a dry period that began on January 20th. However, due to short daylight and reduced vegetation, evapotranspiration was low. As a result, soil moisture decreased slowly and remained sufficient, although some stress was evident as water content exhibited a diurnal cycle. This effect became more pronounced at the end of spring when dry conditions persisted but with high evapotranspiration. Between these two periods, the soil received a significant amount of rain, which promoted substantial grass growth at the site. Rainwater largely remained near the surface, above at least 12 cm depth, with only small quantities infiltrating lower horizons. Only during major rain events (March 8, April 11, and May 7) did water penetrate these horizons and deeper. The significant reductions in soil moisture in the first horizon after rains highlighted the pumping effect of evapotranspiration, as grass roots primarily develop within the top 10 cm of soil.

Instrument data effectively capture the evolution of soil water status during the spring period. A better choice for probe depths would allow two probes to cover the first 15 cm of soil where variation is more important.

Figure 4 presents the variation of soil water amount in each horizon from the soil surface to a depth of 28 cm. Each amount is obtained from moisture data in Figure 3 multiplied by the height of the corresponding horizon. Moisture in the horizon between 8 and 12 cm is inferred from the moisture of adjacent horizons, noting that its height is half that of the other horizons. This presentation of the moisture data in Figure 3 allows for their interpretation in terms of water balance. The last part of the trial shows a significant water deficit developing, more severe than at the trial's start.

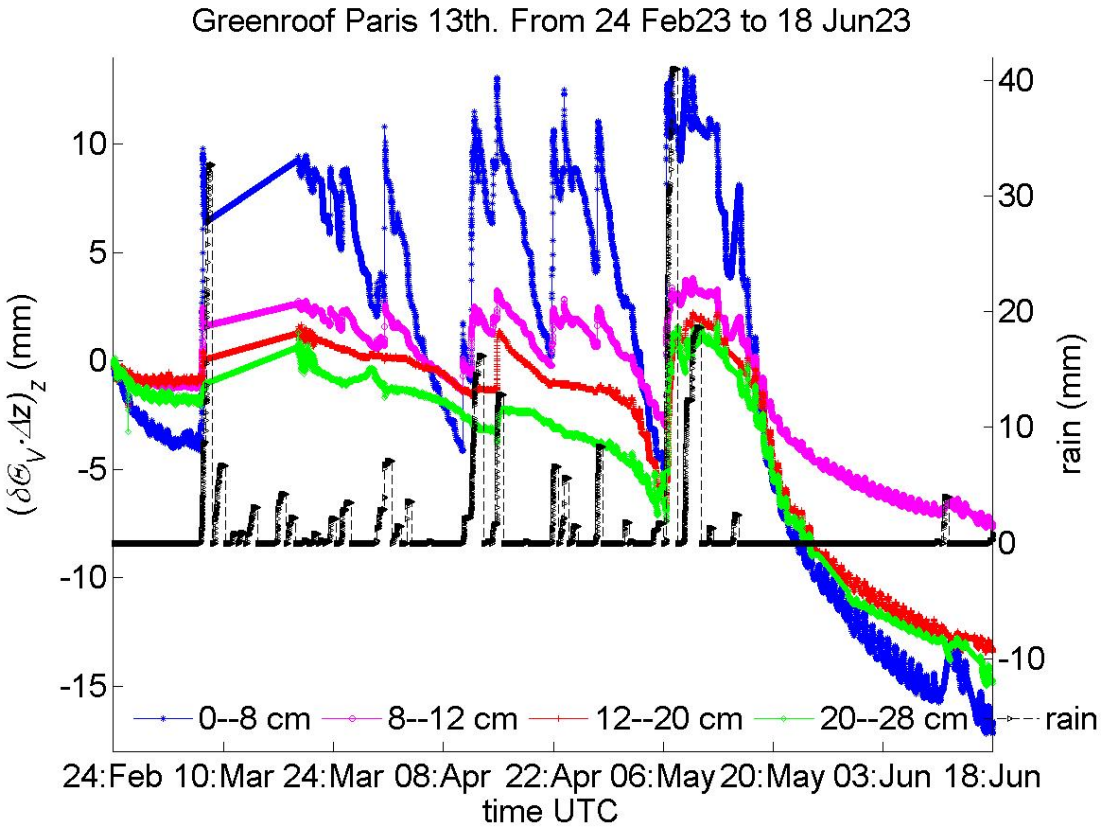

Figure 4. From 24 February, the soil water amount in each horizon probed by the sensor is measured in mm. Each amount is deduced from the soil moisture in Figure 3 multiplied by the horizon height. Moisture in the horizon from 8 to 12 cm corresponds to an average of the moisture in the adjacent horizons. Precipitation for each rain event is also reported.

In Figure 5, the incremental water amounts of the four soil horizons shown in Figure 4 are summed. Cumulative precipitation from 24 February until the trial ends is included for comparison. Until mid-May, the water amount in the sampled soil remained roughly constant with some fluctuations, despite water drainage further down and evapotranspiration, thanks to rains. However, after the end of May, due to a lack of rain, this part of the soil lost an amount of water equivalent to 50 mm relative to the trial start.

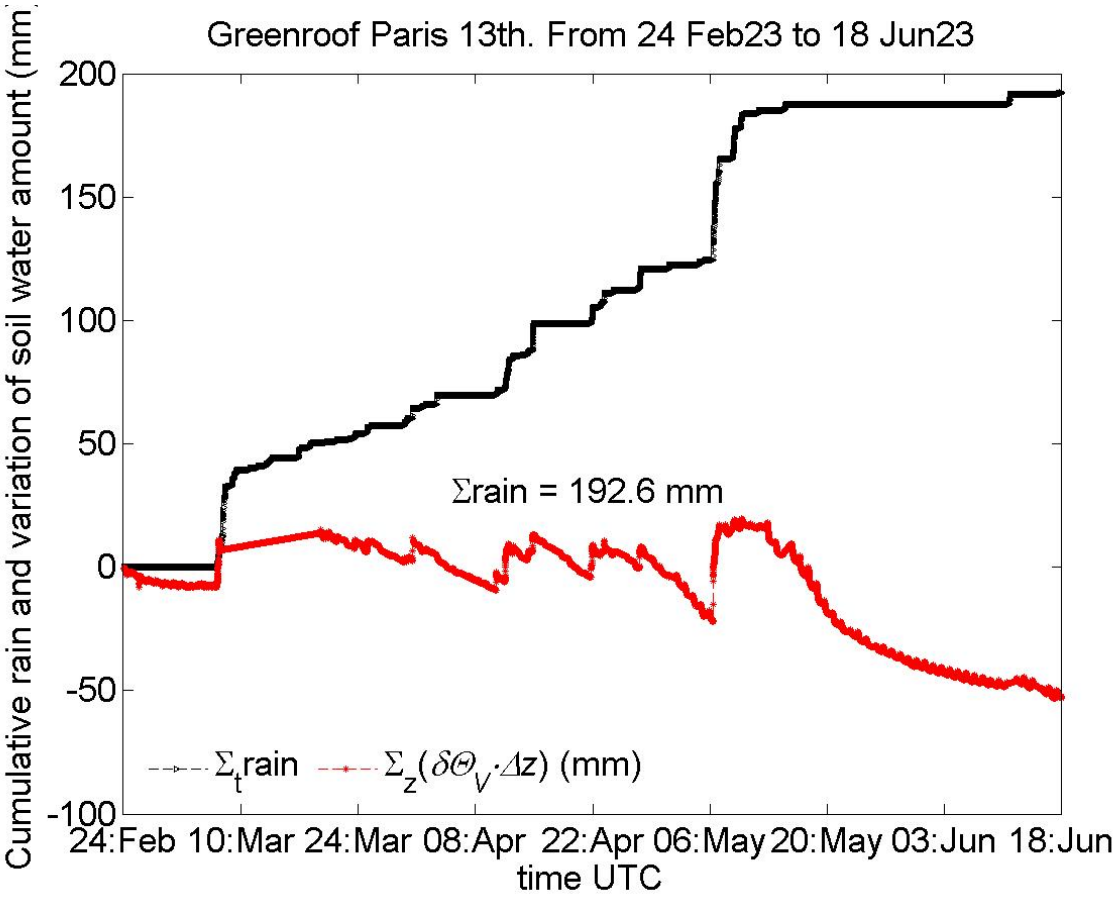

Figure 5. The sum of soil water amounts over the four horizons from the surface, as deduced from Figure 4, is reported against the cumulative precipitation in mm from 24 February to 18 June 2023.

4.2. Soil Conductivity

Figure 6 presents a time series of soil bulk conductivity σ at different horizons as measured by the sensor, i.e., from the imaginary part of the complex permittivity obtained with Equation (3). The quantity depends on the soil moisture and we can observe some similarity with curves in Figure 3. However, there are differences such as a higher sensitivity to rainfalls and to dry conditions as well (a rapid fall of surface bulk conductivity occurred after 16 May). Conductivity σ depends equally on water pore conductivity σ_{ion}, which can change.

An approximation to separate both contributions to σ involves the use of the simple semi-empirical relation proposed by Hilhorst [30,55]:

$$\sigma_{ion} = \frac{\sigma \varepsilon_{r_w}}{\varepsilon_r - \varepsilon_{r(\sigma=0)}}, \quad (5)$$

where ε_{r_w} is the relative permittivity of water at soil temperature.

The function assumes that soil conductivity σ only results from ionic currents in pore water. Dissipation due to dipole relaxations is, thus, neglected. The ratio $(\varepsilon_r - \varepsilon_{r(\sigma=0)})/\varepsilon_{r_w}$ accounts for the water volume fraction in soil, which represents the factor between σ_{ion} and

σ. Hilhorst verified the relation with ε_r measurements on samples at different conductivities σ from its own sensor operating at 20 MHz. The constant $\varepsilon_{r(\sigma=0)}$ represents the asymptotic value of medium permittivity as σ decreases. In the absence of medium calibration, Hilhorst suggested the value $\varepsilon_{r(\sigma=0)} = 4.1$. However, during a dry spell in which ε_r becomes low, field measurements in the case of sandy soil have shown the necessity for a smaller value, 2 or even 1, in order to avoid extreme or negative values of σ_{ion}.

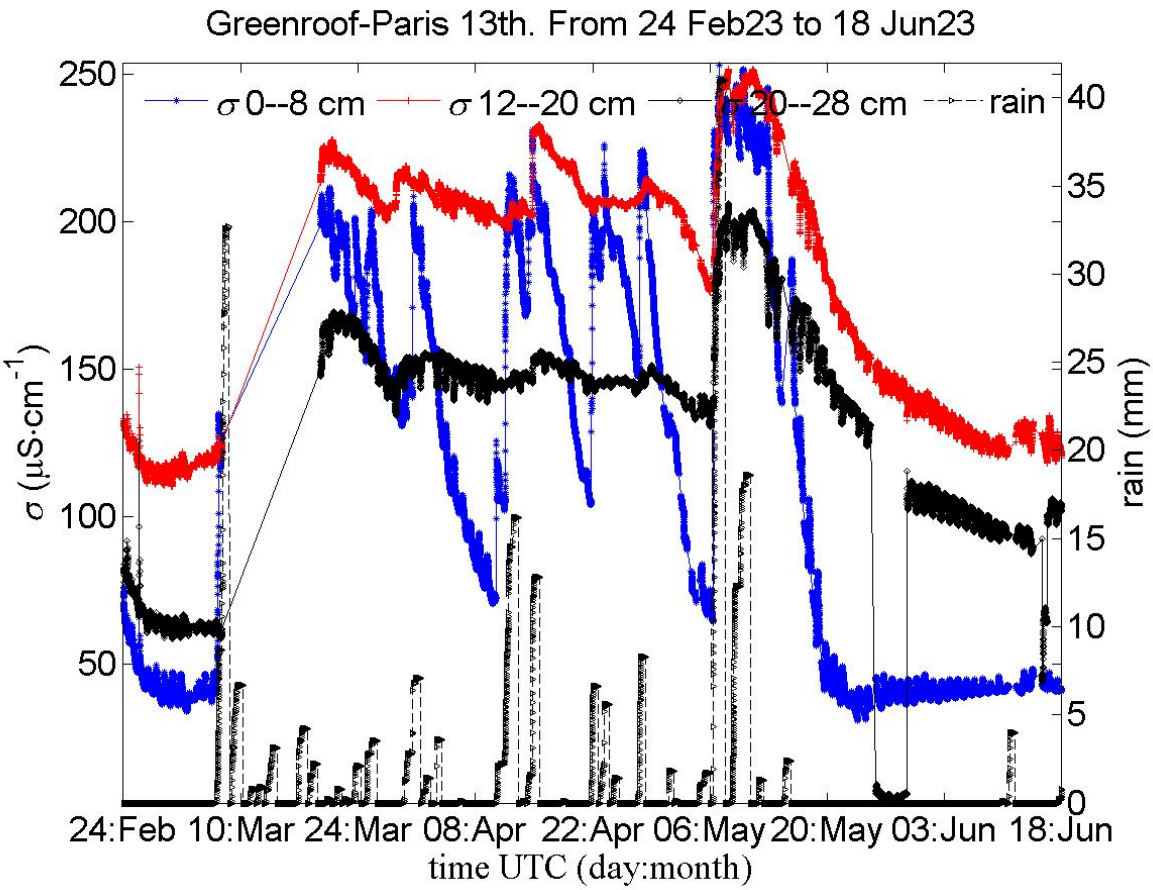

Figure 6. Variation of soil bulk conductivity from 24 February to 18 June 2023 as measured by the device over the three horizons covered by the sensor probes, along with precipitations during the period. One probe was removed at the end of May for a cross-interference test.

The quantity σ_{ion} is controlled by the difference between σ and $\boldsymbol{\varepsilon_r}$. As a consequence, it is very sensitive to any instrument bias or phase error between permittivity and conductivity. Hilhorst suggested restricting the use of Equation (5) to sensors measuring σ and $\boldsymbol{\varepsilon_r}$ simultaneously with the same instrument, that is, directly measuring the complex permittivity like in our case.

Figure 7 results from the application of Equation (5) to times series in Figure 6. Expected values of σ_{ion} are much higher than those for σ. At the same time, they are less sensitive to rainfalls and evaporation. Nonetheless, they often rise with rains, especially σ_{ion} in the horizon close to the surface, despite the fact that rainwater has low conductivity. This can typically be explained by the high dissolution of salt at the surface before deeper water infiltration, coupled with low-salt pore water prior to rainfall. However, there are exceptions, such as the minor rain event on the 16 June following a dry and hot period. In this case, the effect of pore water dilution with rainwater is more significant than salt dissolution. The phenomenon is more common than variations of σ_{ion} over the spring period as shown in Figure 7 (see Section 4.4).

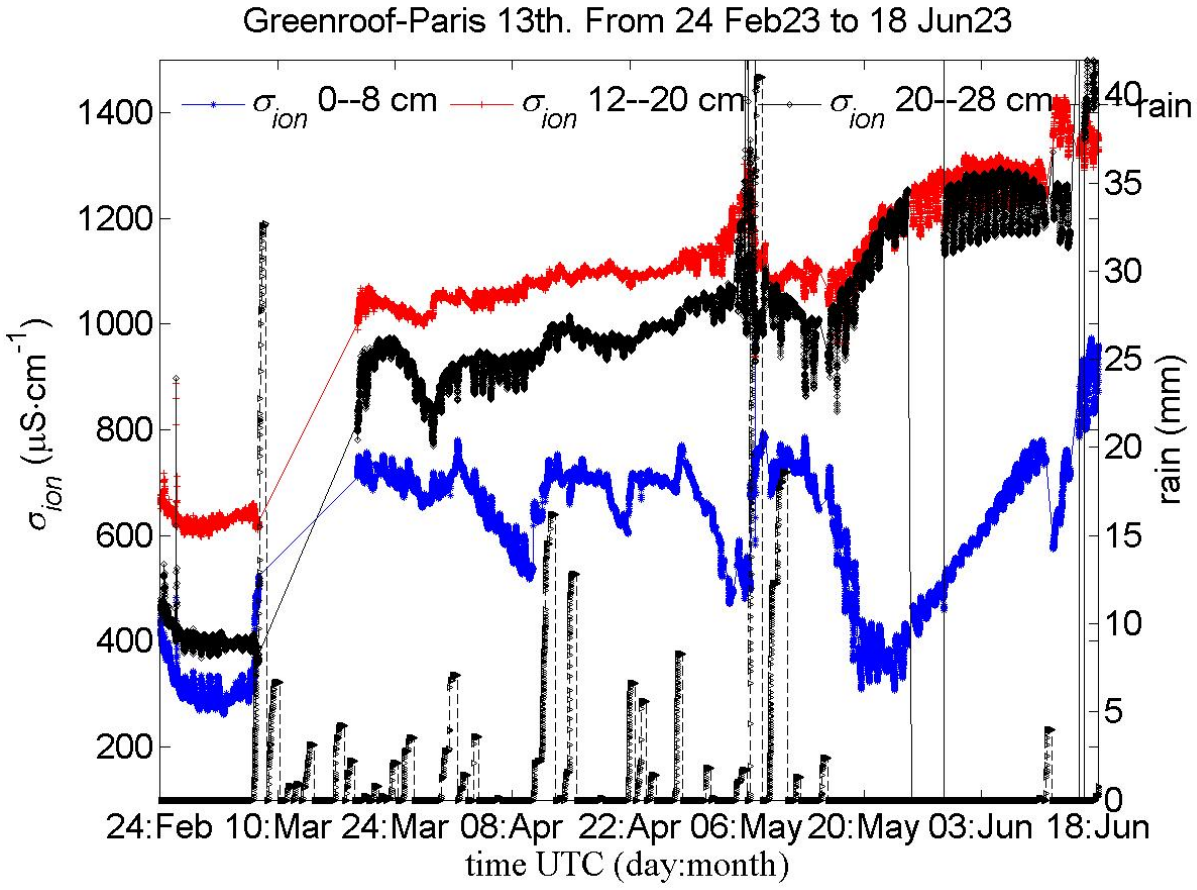

Figure 7. Variations of the conductivity of soil pore water at the three horizons from 24 February to 18 June 2023. They are deduced from data in Figure 6 and their conversion using Equation (5).

The beginning of the dry period was marked by a large decrease in salinity in the shallowest horizon. On the other hand, once a dry spell became acute with grass withering for the lack of soil water, salinity rose. This can be interpreted as a saline concentration of the remaining pore water.

Salt uptake by plants must also be taken into account, complicating data interpretation. As we focus on presenting sensor measurement capabilities, we do not elaborate further, which would require complementary measurements.

Both σ and σ_{ion} exhibit diurnal cycles. These cycles can be partially explained by soil temperature variations, as ionic conductivity is controlled by water viscosity, which depends on temperature.

4.3. Soil Temperature

Figure 8 presents a time series of the soil temperatures at five depths, determined from data collected by device thermocouples. It also reports the electronic temperature from the onboard thermometer. Both diurnal cycles and the rise in soil temperature from winter to summer are visible. The deeper the depth, the less sensitive the soil temperature is to high-frequency changes at the surface, with the soil acting as a low-pass filter. However, at a 50-cm depth, the temperature follows seasonal changes.

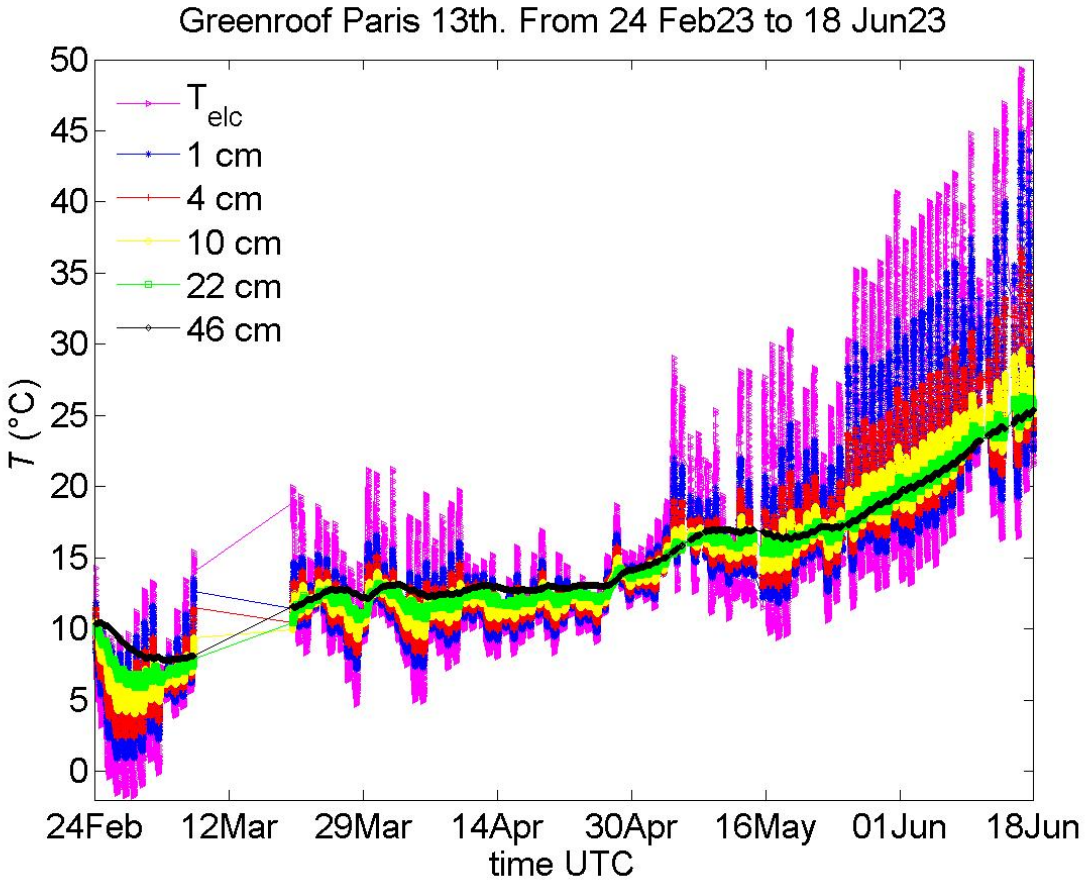

Figure 8. Variations in the soil temperatures at five depths from 24 February to 18 June 2023, measured by the device along the thermocouple stick (see (b) of Figure 1). The temperature on the circuit board, T_{elc} is also recorded.

4.4. Soil MultiVariables at the Horizon

Figure 9 shows variations in the three quantities determined by the sensor in the surface horizon for a two-week interval in April 2023. Dependence between quantities can, thus, be deduced. Furthermore, a major rain event with successive precipitations occurred mid-interval, after several days without rain. Before the rain, salinity was decreasing, and at the same time, presented a good correlation with the diurnal cycles of temperature at the middle depth of the horizon. It was still influenced by the temperature cycles during and after the rain period. As mentioned previously, conductivity depends on water viscosity, which diminishes with temperature. The first two rain events raised the salinity, but it decreased for the subsequent ones. In Figure 7, this difference in behavior with rain is also observed, likely linked to the level of saline concentration before the rain or the soil water content. The content rose each time precipitation occurred, as expected with high soil porosity. The increase in Θ_v is followed by a rapid decrease due to the soil's high hydrological conductivity. Moisture variation presents a slight diurnal cycle, but its shape differs from the cycles of other variables, with a small phase advance.

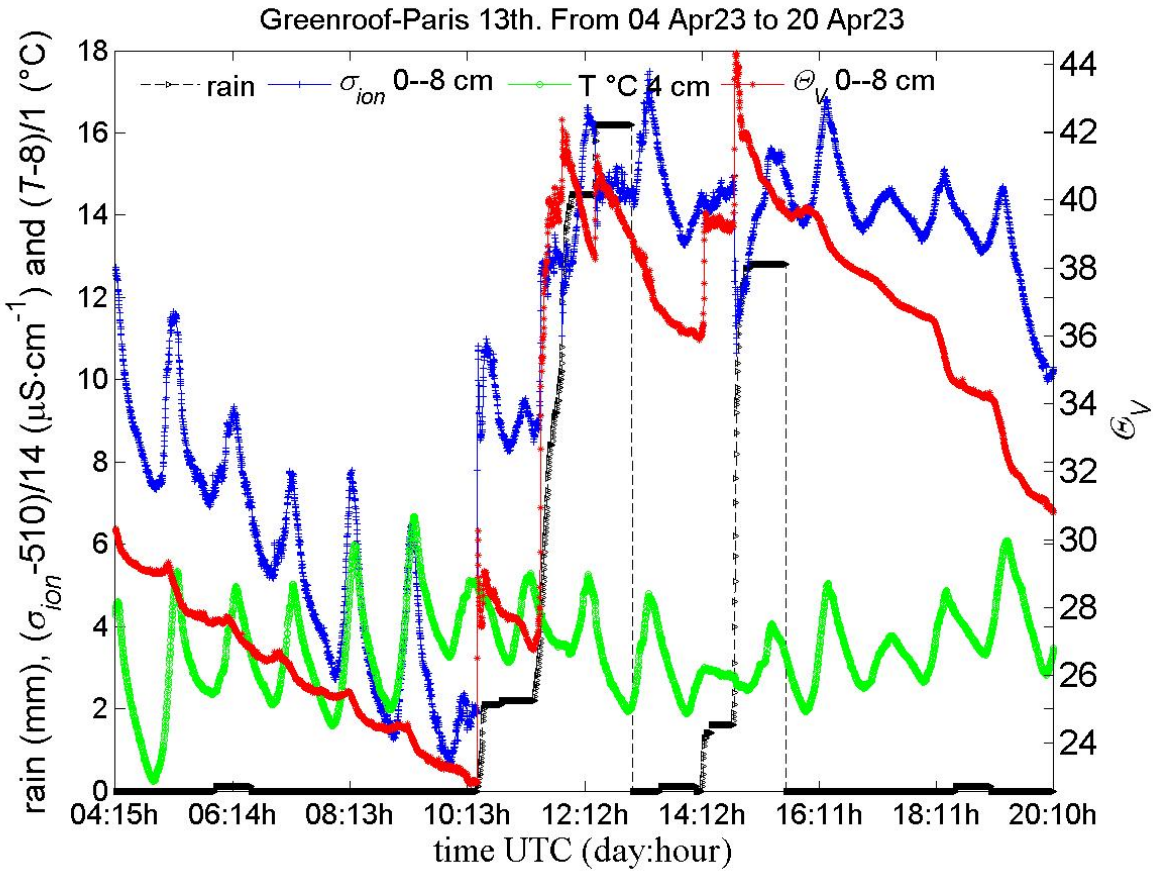

Figure 9. Variation in soil moisture, salinity, and temperature at the horizon close to the surface from 4 to 20 April 2023, as measured by the device. Temperature is measured at a 4 cm depth, which corresponds to the middle point of the horizon, while other variables are average. Salinity and temperature have their scale translated and reduced to enhance their variation during the time interval. Rainfalls are also reported.

The graph provides evidence of the differences in behavior between moisture and salinity, which is consistent with their distinct natures. It demonstrates the high-phase resolution of the instrument in measuring soil complex permittivity.

5. Conclusions

This article describes an in situ sensor that we developed to meet the need for continuous monitoring of soil variables along a vertical profile, such as water content, salinity, and temperature. It also reviews existing in situ soil sensors and wireless networks of these sensors, identifying gaps that need to be addressed. This article demonstrates that our device meets the highest quality of measurement, even surpassing TDR sensors, as its measurement technique provides high phase resolution to output soil complex permittivity. This quantity allows for the determination of soil water content and salinity using conversion formulae that are independent of the instrument. Additionally, the sensor minimizes any perturbation to water flows above and below ground to ensure representativeness.

Some results presented in this article demonstrate the sensor's unique capabilities, particularly in determining soil salinity, which varies consistently with temperature and rainfall.

At the same time, thanks to high electronic integration, compactness, and the choice of components, costs have been reduced for series production. These costs include fabrication, field installation, maintenance, and quality control. The device is designed to be autonomous in terms of operation, communication, and energy for more than one year, utilizing recent technologies like LoRaWAN radio mode. Data are available on a web-accessed

database in real time. These characteristics will enable the construction of wireless, autonomous networks of in situ soil sensors for multi-horizon and multivariable monitoring over large areas. The probe's modular design also allows for less stringent applications, such as monitoring the process or aging of concrete, or the maturing of compost, etc.).

Author Contributions: X.C. performed the experiments, analyzed the data, and wrote most of the paper; X.C. and J.-P.F. conceived and designed the experiments; J.-P.F. initiated the research on the sensor. All authors have read and agreed to the published version of the manuscript.

Funding: This research is part of the program "TERRA FORMA" funded by grant 21-ESRE-0014 of the Agence Nationale de la Recherche. It answered the calls to submit projects to the "2020 Facilities of Excellence" competition named EquipEx+.

Data Availability Statement: The original contributions presented in the study are included in the article, further inquiries can be directed to the corresponding author on reasonable request.

Conflicts of Interest: The authors declare no conflicts of interest.

References

1. Robinson, D.; Campbell, C.; Hopmans, J.; Hornbuckle, B.; Jones, S.; Knight, R.; Ogden, F.; Selker, J.; Wendroth, O. Soil moisture measurement for ecological and hydrological watershed-scale observatories: A review. *Vadose Zone J.* **2008**, *7*, 358. [CrossRef]
2. Seneviratne, S.I.; Corti, T.; Davin, E.L.; Hirschi, M.; Jaeger, E.B.; Lehner, I.; Orlowsky, B.; Teuling, A.J. Investigating soil moisture–climate interactions in a changing climate: A review. *Earth-Sci. Rev.* **2010**, *99*, 125–161. [CrossRef]
3. Brocca, L.; Ciabatta, L.; Massari, C.; Camici, S.; Tarpanelli, A. Soil moisture for hydrological applications: Open questions and new opportunities. *Water* **2017**, *9*, 140. [CrossRef]
4. FAO. *Water for Sustainable Food and Agriculture a Report Produced for the G20 Presidency of Germany*; FAO: Rome, Italy, 2017.
5. FAO. *The State of Food and Agriculture 2020. Overcoming Water Challenges in Agriculture*; Technical Report; FAO: Rome, Italy, 2020.
6. Sauer, T.J.; Horton, R. Soil heat flux. *Micrometeorol. Agric. Syst.* **2005**, *47*, 131–154.
7. Calvet, J.C.; Fritz, N.; Berne, C.; Piguet, B.; Maurel, W.; Meurey, C. Deriving pedotransfer functions for soil quartz fraction in southern France from reverse modeling. *Soil* **2016**, *2*, 615. [CrossRef]
8. Krzeminska, D.M.; Steele-Dunne, S.C.; Bogaard, T.A.; Rutten, M.M.; Sailhac, P.; Geraud, Y. High-resolution temperature observations to monitor soil thermal properties as a proxy for soil moisture condition in clay-shale landslide. *Hydrol. Process.* **2012**, *26*, 2143–2156. [CrossRef]
9. Roux, N.; Costard, F.; Grenier, C. Laboratory and Numerical Simulation of the Evolution of a River's Talik. *Permafr. Periglac. Process.* **2017**, *28*, 460–469. [CrossRef]
10. Rhoades, J.; Chanduvi, F.; Lesche, S. *Soil Salinity Assessment: Methods and Interpretation of Electrical Conductivity Measurements*; FAO: Rome, Italy, 1999; Volume 57, p. 156.
11. Makul, N. Dielectric permittivity of various cement-based materials during the first 24 hours hydration. *Open J. Inorg.-Non-Met. Mater.* **2013**, *2013*, 37922. [CrossRef]
12. Cai, L.; Chen, T.B.; Gao, D.; Liu, H.T.; Chen, J.; Zheng, G.D. Time domain reflectometry measured moisture content of sewage sludge compost across temperatures. *Waste Manag.* **2013**, *33*, 12–17. [CrossRef]
13. Hardie, M. Review of Novel and Emerging Proximal Soil Moisture Sensors for Use in Agriculture. *Sensors* **2020**, *20*, 6934. [CrossRef]
14. Zreda, M.; Shuttleworth, W.; Zeng, X.; Zweck, C.; Desilets, D.; Franz, T.; Rosolem, R. COSMOS: The cosmic-ray soil moisture observing system. *Hydrol. Earth Syst. Sci.* **2012**, *16*, 4079–4099. [CrossRef]
15. Wang, L.; Qu, J.J. Satellite remote sensing applications for surface soil moisture monitoring: A review. *Front. Earth Sci. China* **2009**, *3*, 237–247. [CrossRef]
16. Pramanik, M.; Khanna, M.; Singh, M.; Singh, D.; Sudhishri, S.; Bhatia, A.; Ranjan, R. Automation of soil moisture sensor-based basin irrigation system. *Smart Agric. Technol.* **2022**, *2*, 100032. [CrossRef]
17. Wang, N.; Zhang, N.; Wang, M. Wireless sensors in agriculture and food industry—Recent development and future perspective. *Comput. Electron. Agric.* **2006**, *50*, 1–14. [CrossRef]
18. Bogena, H.; Herbst, M.; Huisman, J.; Rosenbaum, U.; Weuthen, A.; Vereecken, H. Potential of wireless sensor networks for measuring soil water content variability. *Vadose Zone J.* **2010**, *9*, 1002–1013. [CrossRef]
19. Mekki, K.; Bajic, E.; Chaxel, F.; Meyer, F. Overview of cellular LPWAN technologies for IoT deployment: Sigfox, LoRaWAN, and NB-IoT. In Proceedings of the 2018 IEEE International Conference on Pervasive Computing and Communications Workshops (Percom Workshops), Athens, Greece, 19–23 March 2018; pp. 197–202.
20. Chavanne, X.; Frangi, J.P. Smart networks of autonomous in-situ soil sensors. *Eur. J. Environ. Civ. Eng.* **2023**, *27*, 3343–3362. [CrossRef]
21. DFROBOT Capacitive Soil Moisture Sensor SKU:SEN0193 v.1.0. Available online: https://wiki.dfrobot.com/Capacitive_Soil_Moisture_Sensor_SKU_SEN0193 (accessed on 20 March 2024).

22. Reynolds, S. The gravimetric method of soil moisture determination. *J. Hydrol.* **1970**, *11*, 258–300. [CrossRef]
23. Chelidze, T.L.; Gueguen, Y.; Ruffet, C. Electrical spectroscopy of porous rocks: A review I. Theoretical models. *Geophys. J. Int.* **1999**, *137*, 16–34. [CrossRef]
24. Descarpentries, M. *Contribution à L"étude de la Conductivité et de la Polarisation Complexe dans les Milieux Hétérogènes Sable-Argile-Eau*; Technical Report; Institut Français du Pétrole: Paris, France, 1966.
25. Campbell, J.E. Dielectric properties and influence of conductivity in soils at one to fifty megahertz. *Soil Sci. Soc. Am. J.* **1990**, *54*, 332–341. [CrossRef]
26. Eller, H.; Denoth, A. A capacitive soil moisture sensor. *J. Hydrol.* **1996**, *185*, 137–146. [CrossRef]
27. Kessouri, P. Mesure Simultanée aux Fréquences Moyennes et Cartographie de la Permittivité Diélectrique et de la Conductivité Électrique du sol. Ph.D. Thesis, Université Pierre et Marie Curie-Paris VI, Paris, France, 2012.
28. Revil, A. Effective conductivity and permittivity of unsaturated porous materials in the frequency range 1 mHz–1GHz. *Water Resour. Res.* **2013**, *49*, 306–327. [CrossRef] [PubMed]
29. Topp, G.; Davis, J.; Annan, A. Electromagnetic determination of soil water content: Measurements in coaxial transmission lines. *Water Resour. Res.* **1980**, *16*, 574–582. [CrossRef]
30. Hilhorst, M. Dielectric Characterisation of Soil. Ph.D. Thesis, Agricultural University of Wageningen, Wageningen, The Netherlands, 1998.
31. Bechtold, M.; Huisman, J.; Weihermüller, L.; Vereecken, H. Accurate determination of the bulk electrical conductivity with the TDR100 cable tester. *Soil Sci. Soc. Am. J.* **2010**, *74*, 495–501. [CrossRef]
32. Jones, S.B.; Blonquist, J.; Robinson, D.; Rasmussen, V.P.; Or, D. Standardizing characterization of electromagnetic water content sensors. *Vadose Zone J.* **2005**, *4*, 1048–1058. [CrossRef]
33. Chavanne, X.; Frangi, J.P. Monitoring soil water content and its salinity with high-precision and low-cost in-situ sensors. *Eur. J. Environ. Civ. Eng.* **2023**, *27*, 457–478. [CrossRef]
34. Jackson, J.D. *Classical Electrodynamics*, 3rd ed.; Wiley-VCH: Weinheim, Germany, 1998; Chapter 5, p. 832, ISBN 0-471-30932-X.
35. Wilson, T.B.; Kochendorfer, J.; Diamond, H.J.; Meyers, T.P.; Hall, M.; French, B.; Myles, L.; Saylor, R.D. A field evaluation of the SoilVUE10 soil moisture sensor. *Vadose Zone J.* **2023**, *22*, e20241. [CrossRef]
36. Campbell Scientific, Inc. *SoilVUETM10 Manual*; Campbell Scientific, Inc.: Logan, UT, USA, 2019.
37. Qu, W.; Bogena, H.; Huisman, J.A.; Vereecken, H. Calibration of a novel low-cost soil water content sensor based on a ring oscillator. *Vadose Zone J.* **2013**, *12*, 1–10. [CrossRef]
38. Campbell Scientific, Inc. *CS650 and CS655 Water Content Reflectometers Manual*; Campbell Scientific, Inc.: Logan, UT, USA, 2016.
39. Kim, H.; Cosh, M.H.; Bindlish, R.; Lakshmi, V. Field evaluation of portable soil water content sensors in a sandy loam. *Vadose Zone J.* **2020**, *19*, e20033. [CrossRef]
40. Bogena, H.R.; Huisman, J.A.; Schilling, B.; Weuthen, A.; Vereecken, H. Effective calibration of low-cost soil water content sensors. *Sensors* **2017**, *17*, 208. [CrossRef]
41. Wild, J.; Kopecký, M.; Macek, M.; Šanda, M.; Jankovec, J.; Haase, T. Climate at ecologically relevant scales: A new temperature and soil moisture logger for long-term microclimate measurement. *Agric. For. Meteorol.* **2019**, *268*, 40–47. [CrossRef]
42. Kelleners, T.; Soppe, R.; Robinson, D.; Schaap, M.; Ayars, J.; Skaggs, T. Calibration of capacitance probe sensors using electric circuit theory. *Soil Sci. Soc. Am. J.* **2004**, *68*, 770–778. [CrossRef]
43. Chavanne, X.; Bruère, A.; Frangi, J.P. Comments to: A Novel Low-Cost Instrumentation System for Measuring the Water Content and Apparent Electrical Conductivity of Soils, Sensors, 15, 25546–25563. *Sensors* **2018**, *18*, 1730. [CrossRef] [PubMed]
44. Gaskin, G.; Miller, J. Measurement of soil water content using a simplified impedance measuring technique. *J. Agric. Eng. Res.* **1996**, *63*, 153–159. [CrossRef]
45. Bogena, H.; Huisman, J.; Oberdörster, C.; Vereecken, H. Evaluation of a low-cost soil water content sensor for wireless network applications. *J. Hydrol.* **2007**, *344*, 32–42. [CrossRef]
46. Peddinti, S.R.; Hopmans, J.W.; Abou Najm, M.; Kisekka, I. Assessing effects of salinity on the performance of a low-cost wireless soil water sensor. *Sensors* **2020**, *20*, 7041. [CrossRef]
47. Placidi, P.; Gasperini, L.; Grassi, A.; Cecconi, M.; Scorzoni, A. Characterization of low-cost capacitive soil moisture sensors for IoT networks. *Sensors* **2020**, *20*, 3585. [CrossRef] [PubMed]
48. gikfun Capacitive Soil Moisture Sensor EK1940-17 v.1.2. Available online: https://gikfun.com/products/gikfun-capacitive-soil-moisture-sensor-corrosion-resistant-for-arduino-moisture-detection-garden-watering-diy-pack-of-2pcs (accessed on 20 March 2024).
49. Chavanne, X.; Frangi, J.P. Sample volume of a capacitance moisture sensor in function of its geometry. *Eur. J. Environ. Civ. Eng.* **2020**, *24*, 2168–2186. [CrossRef]
50. Rosenbaum, U.; Huisman, J.; Vrba, J.; Vereecken, H.; Bogena, H. Correction of temperature and electrical conductivity effects on dielectric permittivity measurements with ECH2O sensors. *VAdose Zone J.* **2011**, *10*, 582–593. [CrossRef]
51. Chavanne, X.; Bruère, A.; Frangi, J.P. Study of fringe effects of a two-rod capacitor embedded in a medium in order to deduce its permittivity. *Eur. J. Environ. Civ. Eng.* **2020**, *26*, 2439–2452. [CrossRef]
52. Chavanne, X.; Frangi, J.P. Presentation of a Complex Permittivity-Meter with Applications for Sensing the Moisture and Salinity of a Porous Media. *Sensors* **2014**, *14*, 15815–15835.

53. Burns, G.W.; Scroger, M.G.; Strouse, G.F.; Croarkin, M.C.; Guthrie, W.F. *Temperature-Electromotive Force Reference Functions and Tables for the Letter-Designated Thermocouple Types Based on the ITS-90*; NASA STI/Recon Technical Report N; National Institute of Standards and Technology: Gaithersburg, MD, USA, 1993; Volume 93, p. 31214.
54. Johansen, O. *Thermal Conductivity of Soils*; Draft Translation in English; Technical Report; Cold Regions Research and Engineering Lab.: Hanover NH, USA, 1977.
55. Hilhorst, M. A pore water conductivity sensor. *Soil Sci. Soc. Am. J.* **2000**, *64*, 1922–1925. [CrossRef]